ORIGINAL PAPER

Spatial analysis of the frequency–magnitude distribution of aftershock activity of 2003 Bam earthquake: southeast Iran

Behnam Rahimi

Abstract The Bam earthquake (2003 December 26, $M_W = 6.6$) was one of the largest earthquakes that occurred in southeast of Iran during last century. It took place along an N–S trending right-lateral strike-slip fault, almost near the southern end of Nyband–Gowk fault. In this study, we mapped the frequency–magnitude distribution of aftershock events spatially across the Bam aftershock zone. The b-value varies between 0.6 and 1.1 across the Bam rupture zone. The overall depth distribution of b-value in Bam aftershock zone reveals two distinct increases in b-value: (1) at depths of 8–10 km and (2) shallower than 4 km beneath the Bam city. There is no correlation between high b-value anomalies found in this study and the region of largest slip, whereas the spatial correlation between high b-value anomalies and the zone of low V_s and high σ (in earlier tomography study) is obvious. This correlation reveals that material properties and increasing heterogeneity are more important in controlling b-value distribution in Bam earthquake rupture zone. The high b-value anomaly near the surface of northern part of rupture zone may be related to unconsolidated and water-rich quaternary alluvial sediments and probable low-strength rocks beneath them. The high b-value anomaly at depth range 8–10 km can be correlated with fractured and fluid-filled mass, which may result from the movement of magma during Eocene volcanism in the Bam area. In this study, the induced changes in pore fluid pressure due to main shock are suggested as a mechanism for aftershock generation.

Keywords Bam earthquake · b-Value · Iran

B. Rahimi (✉)
Department of Geology, Earthquake Research Centre,
Ferdowsi University of Mashhad, Mashhad, Iran
e-mail: b-rahimi@ferdowsi.um.ac.ir

Introduction

The frequency–magnitude distribution (FMD) of earthquakes was first introduced by Ishimoto and Iida (1939) in Japan and subsequently in the United States by Gutenberg and Richter (1954). The frequency–magnitude distribution (FMD) is described by the following relation:

$$LogN = a - bM \qquad (1)$$

where N is the cumulative number of events with magnitude larger than M; a and b are constants. a describes the seismic activity of the area, and b indicates the size distribution of events in a region. The estimated coefficient of b which is known as b-value is the most important parameter to characterize seismicity of a region.

The b-value represents the statistical abundance of large and small earthquakes in a sequence of events. The high b-value shows the abundance of events with small magnitude, whereas the low b-value reveals the abundance of large magnitudes. This parameter is related to tectonic characteristics of a region and mostly varies between 0.6 and 1.4 (Wiemer and Katsumata 1999). Many factors can cause variation of b-value from its normal value about 1.0. Increasing material heterogeneity or crack density results in high b-value (Mogi 1962), and increasing in applied shear stress (Scholz 1968) or increasing in effective stress (Wyss 1973) decreases the b-value. Increase in thermal gradient may also cause an increase in b-value (Warren and Latham 1970).

Studying the spatial distribution of b-value in volcanic areas shows an increase in b-value near magma chambers and cracked volumes in crust (e.g. Wiemer and McNutt 1997; Wiemer et al. 1998, 2002).

In this communication, an attempt has been made to study the spatial variation of magnitude–frequency

distribution in aftershock zone of the Bam earthquake of December 26, 2003, Kerman province, central Iran. The variation of magnitude–frequency distribution is studied by b-value mapping in 2D and 3D spaces.

Bam earthquake and its tectonic setting

The current deformation of Iran results from the convergence of the Arabian and Eurasian plates (Walker and Jackson 2002). GPS measurements show that the Arabia moves 21–25 mm/year due north relative to Eurasia (Vernant et al. 2004). This convergence is partitioned into collision-oblique and collision-parallel seismic belt in Iran (Jackson et al. 1995; Walker and Jackson 2002).

The Bam region is located on the Southwest of the Lut block (Fig. 1). The Lut block is bounded on both eastern and western sides by N–S trending right-lateral strike-slip faults. The Nayband–Gowk fault system bounded the west side of the Lut block. The northern part of this fault system (between ∼33N and 30N), which is known as Nayband fault, had a slip rate equal to 2 mm/year in its late quaternary activity (Walker and Jackson 2002). Between 30N and 29.5N, the strike of the fault system changes to NNW–SSE (Fig. 1). This segment that is the most active fault in southeastern part of Central Iran is called Gowk fault. Five

destructive earthquakes with magnitude M_w 5.4–7 have occurred along this fault since 20 years ago.

The Bam earthquake of December 26, 2003, occurred near the southern end of the Nayband–Gowk fault system. This event destroyed the old city of Bam and its surroundings with population of about 150,000. During this catastrophe which was the worst event in that year anywhere in the world, 26,271 people were killed and tens of thousands of people injured. The main shock of the Bam earthquake occurred at 1:56:52 UTC and 05:26:52 (local time) on December 26, 2003. Its epicentre was found at 29.004N, 58.337E, depth 10 km and moment magnitude 6.6 (www.usgs.org) (Fig. 1). Teleseismic focal mechanism by several groups (e.g. USGS 2003; Yamanaka 2003) showed a steeply dipping, right-lateral strike-slip movement on an N–S trending fault. The Bam fault (Fig. 2) was known before the earthquake; it is extending along west side of Baravat village and probably has been active during the Pleistocene (Berberian 1976; Hessami et al. 2003). Analysis of seismic data and field observation by some researchers reveal that the main shock of the Bam earthquake had occurred on this fault (e.g. Fu et al. 2004;
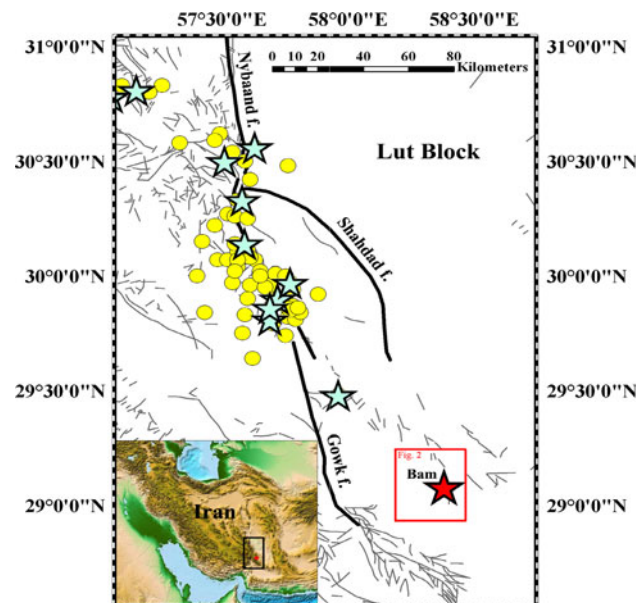

Fig. 1 Tectonic map of the Bam area. Main active faults (*black thick lines*) and minor faults (*grey thin lines*) are shown (fault map available from: www.ngdir.ir). *Yellow circles* are epicenter of earthquakes in the time period 1980–2002 (from Engdahl et al. 1998). The largest instrumental events ($M \geq 4.5$) in the time period 1980–2002 catalogue are plotted as *green stars* (from International Institute of Earthquake Engineering and Seismology of Iran (IEES)). The epicenter of the Bam earthquake is also shown with *red star*. *Red box* shows the area of Fig. 2
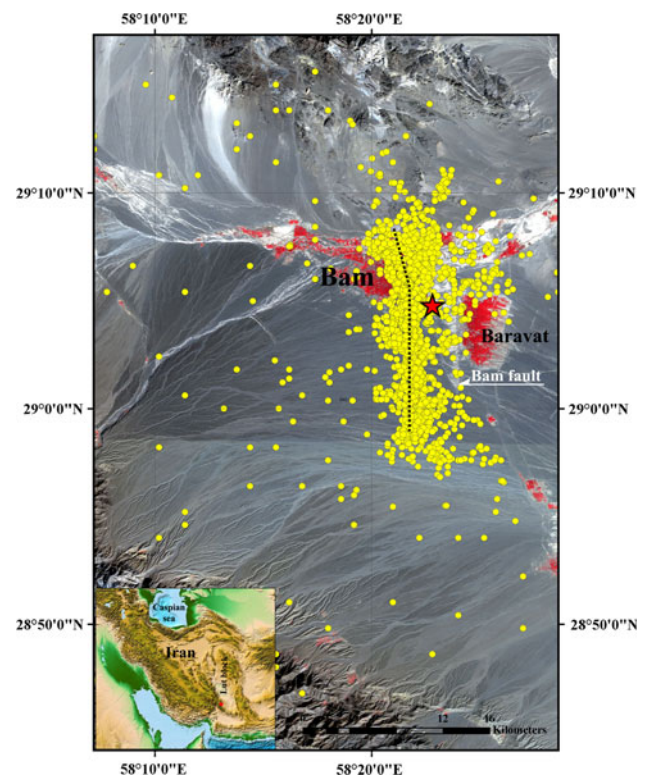

Fig. 2 The epicenter distribution of aftershocks of the Bam earthquake (*yellow circles*) (data from Sadeghi et al. 2006). The epicenter of the Bam earthquake is shown as a *red star*. The Bam fault line escarpment is marked by *arrow* in background, and the inferred seismic fault for the Bam earthquake(Arg-e- Bam fault) is shown by thin *black doted line* (after Nakamura et al. 2005). LANDSAT TM image is available in www.ngdir.ir

Hessami et al. 2003). In contrast, based on the analysis Envisat SAR Interferometry, there are others who believed that the Bam earthquake was caused by a new blind right-lateral strike-slip fault, 5 km west of the Bam fault (Tale-bian et al. 2004; Binet and Bollinger 2005; Fielding et al. 2005).

Nakamura et al. (2005) studied the hypocenter distribution of aftershocks of the Bam earthquake, proposed a schematic 3D structural model for this new fault and have named it "Arge-Bam fault." The spatial distribution of slip on the fault obtained from INSAR shows that the earthquake was a shallow event with the highest slip (2 m) occurring in the depths of 2–8 km (Funning et al. 2005).

Data and method

As seen in other destructive earthquakes, the Bam earthquake was followed by a series of aftershocks. Tatar et al. (2005) studied the Bam aftershock sequence in a period of
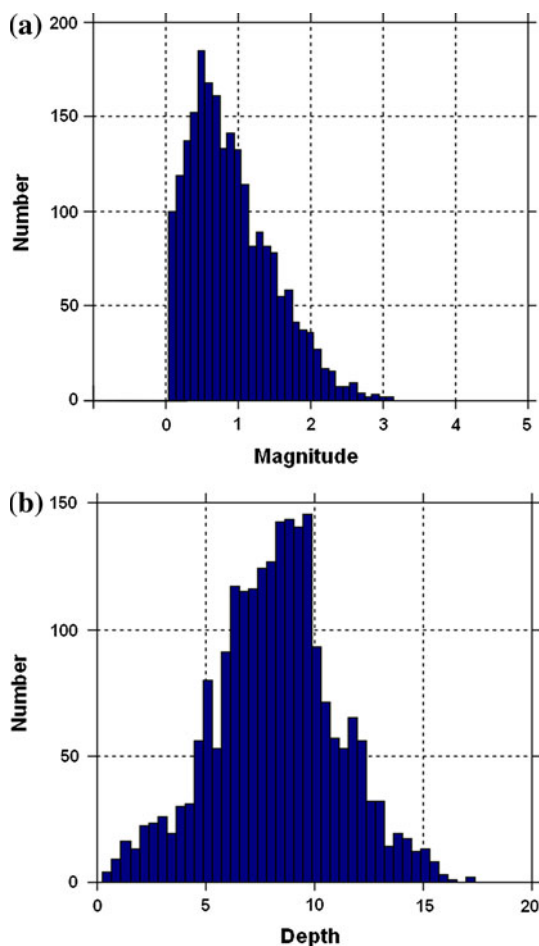

Fig. 3 a Histogram of the number of events versus magnitudes for studied aftershock sequence. **b** Histogram of the number of events versus depths for studied aftershock sequence

3–35 days after the main shock on December 26, 2003. The aftershocks in this period were recorded in a dense seismic network of 23 stations, which was installed in the epicenter area. The second aftershock study was carried out by Nakamura et al. (2005) 41–70 days after the main shock. They used aftershock data, which had been recorded by a seismic network of 9 temporal stations installed in and around the Bam city on February 6, 2004, and recording continued until March 7, 2004. Each station was equipped with a high-sensitive three-component velocity type seis-mometer (LE-3D, Lennartz Electronics) with a normal frequency of 1HZ and a GPS timing system (Suzuki et al. 2004).

Nakamura et al. (2005) used a 1D velocity model and located the aftershock events accurately, and Sadeghi et al. (2006) relocated aftershocks using a 3D velocity model. In this study, the aftershock events of the Bam earthquake in a period of 41–70 days after the main shock (Feb. 6, 2004–March 7, 2004) (Suzuki et al. 2004; Nakamura et al. 2005) are used to evaluate spatial variation of b-value in aftershock zone of Bam earthquake. Among the 2,789 recorded after-shocks, a dataset of 2,396 events that were located accu-rately by Sadeghi et al. (2006) is used. The distribution of aftershocks suggests that the Bam earthquake occurred not in the Bam fault but in the Arg-Bam fault (Fig. 2). The epicentral distribution of aftershocks shows a linear trending 20 km long and 3.5 km west of the Bam fault (Fig. 2). The hypocenter distribution is nearly vertical and dips slightly in the S88 W direction between 0 and 16 km depths (Nakamura et al. 2005). The magnitude of the aftershocks ranged from 0.1 to 3.1 (Fig. 3a). The hypocenter depth of events varies between 0 and 16 km, and the aftershocks with focal depth between 6 and 10 km are abundant (Fig. 3b).

To calculate b-value, the method of maximum likeli-hood with following relation (Aki 1965; Utsu 1992 in Utsu 2002) is used

$$b = \log e / \bar{M} - M_{\min} \qquad (2)$$

where $\bar{M}$ is the average magnitude and $M_{\min}$ is the mag-nitude above which all events recorded in a sequence. It is also referred to as magnitude of completeness (Mc). The estimation of Mc is critical in b-value mapping (Wiemer and Wyss 2000). The magnitude of completeness system-atically varies as a function of space and time. Particularly, the temporal changes can produce erroneous b-value esti-mates (Wiemer and Katsumata 1999). To compute the change in Mc as a function of time in Bam aftershock sequence, we used an overlapping moving window (e.g. Wiemer et al. 1998). In this method, a moving window of 400 events with 50 event increments is used to calculate temporal variation of Mc. Figure 4 shows the variation of Mc through time in the studied aftershock sequence. As shown in this figure, the Mc shows a no constant value
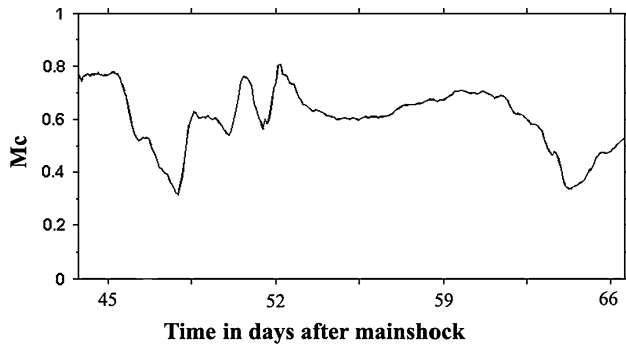
Fig. 4 Plot of *Mc*, the magnitude of completeness with time for the studied aftershock sequence

and varies from 0.3 to 0.8. It may due to change in network quality in data collecting. Figure 5 shows the spatial variation of *Mc* in Bam aftershock zone. The map is computed, using cylindrical volumes with radius *r* equal to 2 km and height equal to 16 km. The center of cylindrical volumes is located at nods with 0.01 degree spacing throughout aftershock zone. As revealed in this Fig. 5, *Mc* is not constant throughout the aftershock region and varies from 0.3 to 0.8. The spatial variations of *Mc* are similar to its temporal variations. Temporal and spatial variations of *Mc* suggest that *Mc* = 0.8 is a good choice and can be selected as minimum magnitude of complete recording in Bam aftershock sequence. Also, plotting of cumulative distribution of events (*M* ≥ 0.8) as a function of time
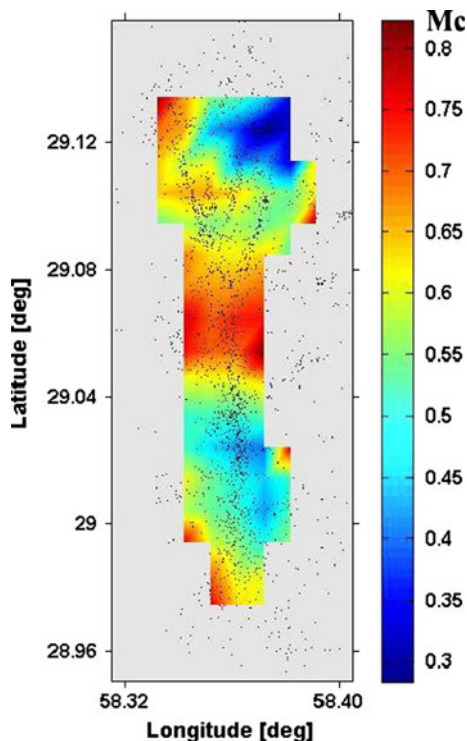

Fig. 5 Surface map of spatial distribution of *Mc* for the Bam aftershock sequence. *Black dots* are epicenters of aftershock events
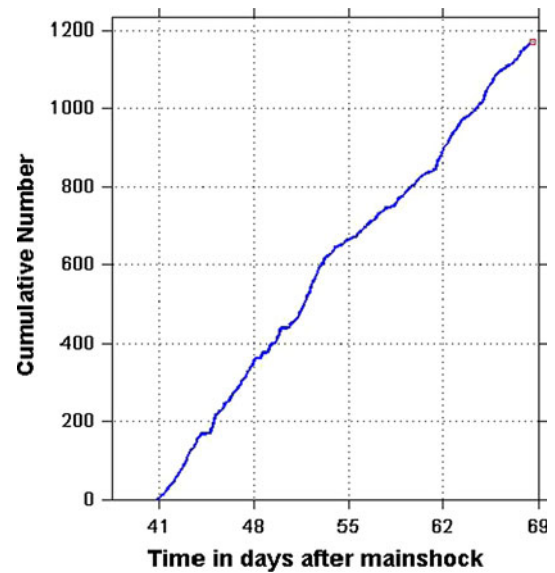

Fig. 6 Cumulative number of aftershocks with magnitude of $M \geq 0.8$ as a function of time for the studied aftershock sequence. The relatively constant slope suggests that this dataset can be accepted as homogenous

shows a nearly constant slope (Fig. 6). It can interpret that the studied dataset is homogenous.

To visualizing the FMD of aftershocks, I used the *b*-value mapping method of Wiemer and Benoit (1996). The method involves setting up a two-dimensional grid over the plane on which the *b*-value variation is to be mapped. This plane can be chosen to be vertical or horizontal. In this study, the *b*-value is calculated at grid nodes that are 1 km apart, on a vertical plane. The *n* = 150 nearest aftershocks are used in each calculation. To estimate the standard deviation of the *b*-value, we used the equation first derived by Aki (1965) and then improved by Shi and Bolt (1982)

$$\partial b = 2.3b^2 \sqrt{\frac{\sum_i (M_i - \bar{M})}{n(n-1)}} \tag{3}$$

where *n* is the sample size and M_i is the magnitude of each event in dataset. All computations are programmed in Zmap software developed by the Wiemer and Zuniga (1994).

Results

Spatial variation of *b*-value across the Bam earthquake rupture zone has been mapped on both horizontal and vertical planes using the maximum likelihood method. Figure 7a shows the *b*-value distribution of the Bam aftershocks, projected on to a vertical N–S trending plane, almost parallel to "Arg-e-Bam fault" (after Nakamura

et al. 2005) (Fig. 7b). As shown in this cross-section, the *b*-value significantly varies in N–S direction as well as the depth. The average *b*-value is fairly low, which is a common characteristic noted in aftershock sequence (Wiemer and Katsumata 1999). The *b*-value varies in the range of 0.6 to 1.1 (Fig. 7a). The standard deviation for *b*-value estimation is, in general, less than 10 percent of calculated *b* (Fig. 8). Four limited areas with relatively high *b*-value were detected and represented by capital letters A, B, C and D (Fig. 7a). To quantify the statistical significance of these anomalous areas, the *P*-test (Utsu 1992) was used

$$P \cong \exp(-(dA/2) - 2) \tag{4}$$

where $dA = -2NLn(N) + 2N_1Ln(N_1 + N_2b_1/b_2) + 2N_2Ln$ $(N_2 + N_1b_2/b_1) - 2$ N_1 and N_2 are the number of events in

the similar spherical volumes to be compared, and $N = N_1 + N_2$. For example, in the anomaly B (circle labeled A in Fig. 9a), $N_1 = 121$ and the resulting $b = 0.91$, and for the background area (circle labeled B in Fig. 9a), $N_2 = 119$ and $b = 0.65$. These values lead to a *P* value equal to 0.012, suggesting that the probability that the two contrasting areas have the same population is low (Fig. 9b). The shallower anomaly A, with $b > 0.95$, and the anomaly patch B, with $b \approx 1.0$, are located in the northern part (zone I in Fig. 7b), beneath the Bam city. The overall *b*-value in this region is equal to 0.78 (Fig. 10a). Anomaly A is located at a depth range 2–4 km, and anomaly B is found at a depth range 8–9 km just beneath the anomaly A. The overall depth distribution of *b*-value in northern part of Bam aftershock zone shows two marked
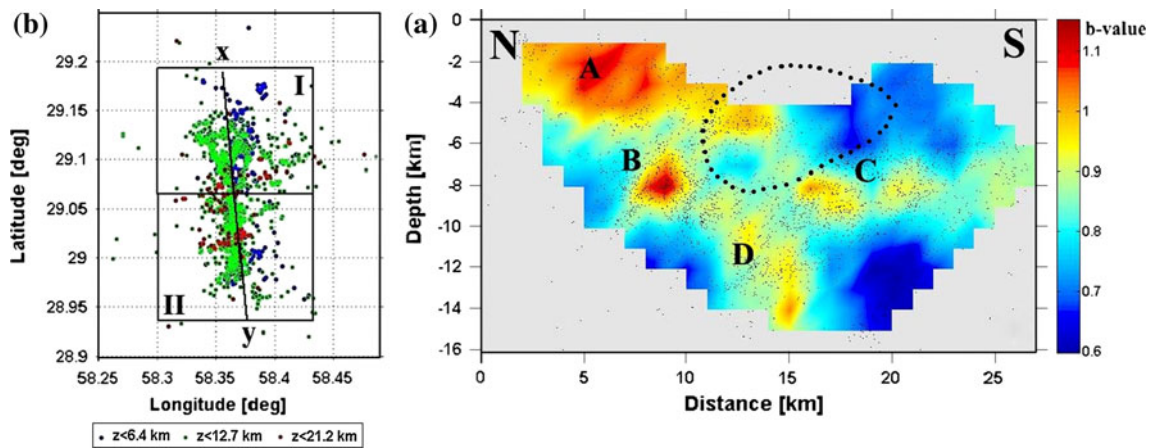

Fig. 7 a Distribution of *b*-value along the Bam earthquake rupture zone (for location see Fig. 7b). The high *b*-value anomalies, named with A, B, C and D, are colored *red*, and the low *b*-values are blue. The area with a slip larger than 2 (m) in the main shock is marked with doted line (after Funning et al. 2005). *Black dots* represent the location of aftershock events (data from Sadeghi et al. 2006). **b** Spatial distribution of aftershock events. The *xy line* shows the strike of cross-section in Fig. 7a

Fig. 8 Spatial variation of standard deviation of calculated *b*-value along the Bam earthquake rupture zone. *Black dots* represent the location of aftershock events (data from Sadeghi et al. 2006)
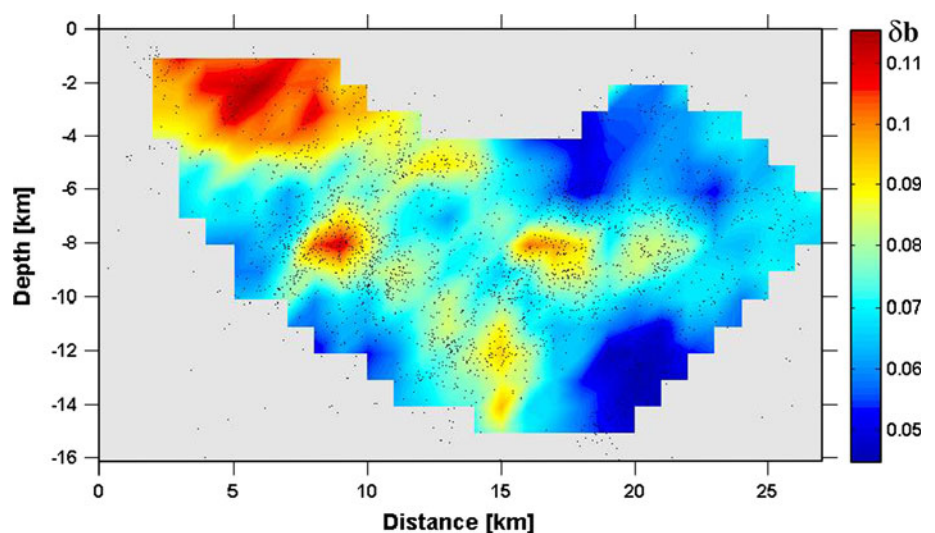
Fig. 9 **a** The *b*-value
distribution on an N–S vertical
cross-section along the Bam
earthquake rupture zone
(described in Fig. 7a). The
circles labeled *A* and *B* enclosed
samples for which *b*-values are
compared. **b** FMD for selected
samples in *A* circle (*white
squares*) and *B* circle (*black
dots*). The value of *P* signals
that the two *b*-value samples are
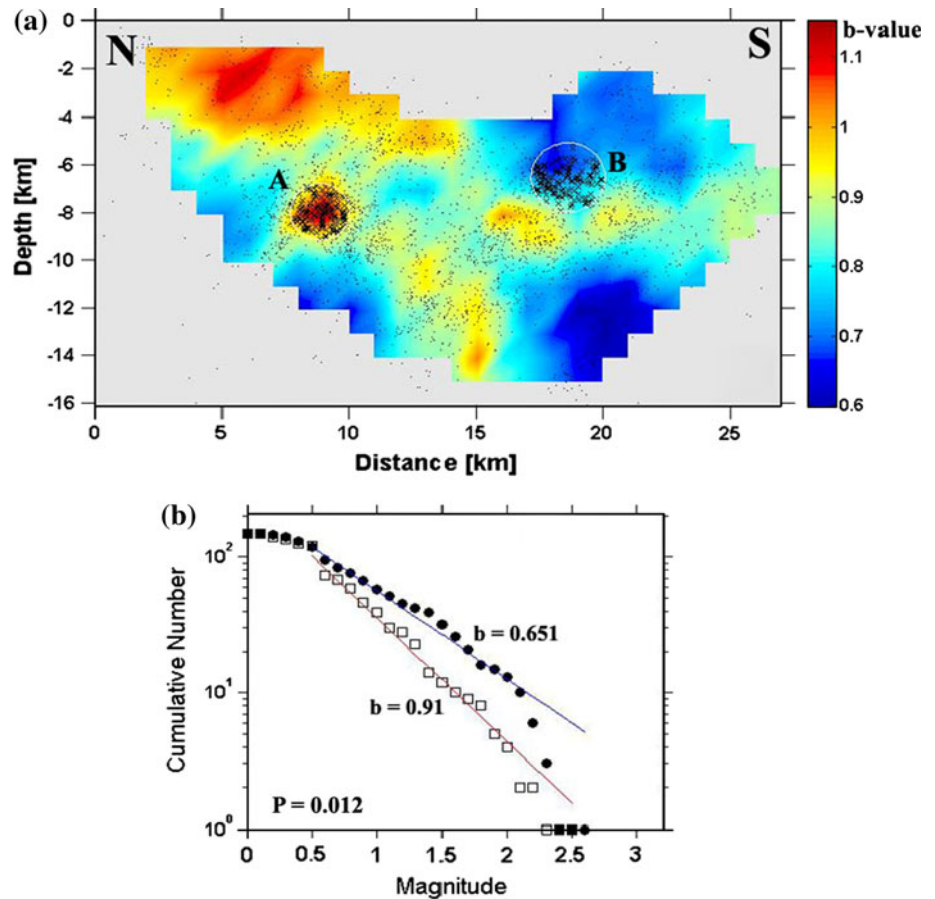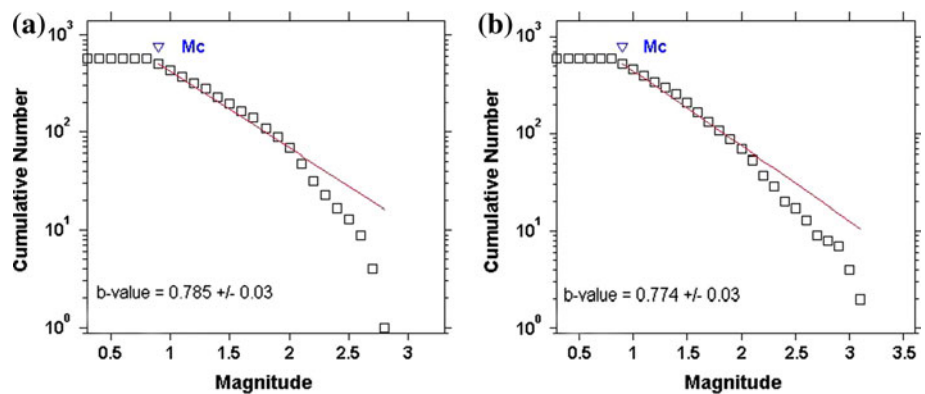significant at the 95%
confidence limit

Fig. 10 The magnitude–
frequency distribution for
selected volumes. **a** The
northern half of the Bam
aftershock zone (zone *I* in
Fig. 7b). **b** The southern half of
the Bam aftershock zone (zone
II in Fig. 7b)

increases in *b*-value (1) shallower than 4 km and (2) at a
depth range of 8 to 10 km. These are distinctly related to A
and B anomalies (Fig. 11a).

The C anomaly is situated at 10 km south of anomaly B
at a same depth. The *b*-value in this anomaly is 0.95. The
final patch of high *b*-value and the deepest one (D) with
$b \approx 0.95$ is located between anomaly B and C, at a depth
range of 10 to 13 km. These anomalies are located in
southern part of bam aftershock zone (zone II in Fig. 7b).
The overall *b*-value in this part is about 0.77 (Fig. 10b).
Figure 11b shows the overall depth distribution of *b*-value

in this zone. This graph suggests a distinct increase in *b*-
value at depths of 8 to 10, which can be related to anomaly
C. The three-dimensional view of high *b*-value anomalies
is shown in Fig. 12.

Discussion

Studying of *b*-value variation in an aftershock sequence has
provided useful information to explain rupture mechanism
and material properties of an earthquake area. The

Fig. 11 plot of Average b-value versus depth for selected volumes. We used sliding windows with 100 events in each, stepping 10 events. *Black squares* show the centre of sliding window, *horizontal lines* show standard deviation and the *vertical lines* show the window size. **a** The northern half of the Bam aftershock zone (zone *I* in Fig. 7b). **b** The southern half of the Bam aftershock zone (zone *II* in Fig. 7b)
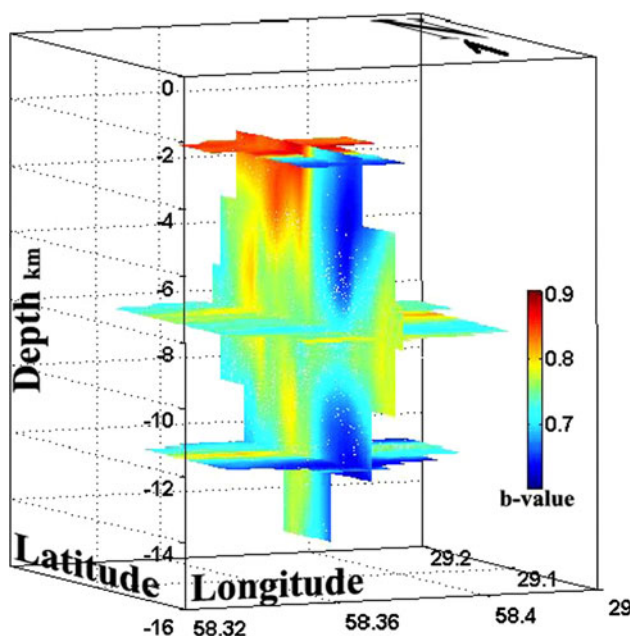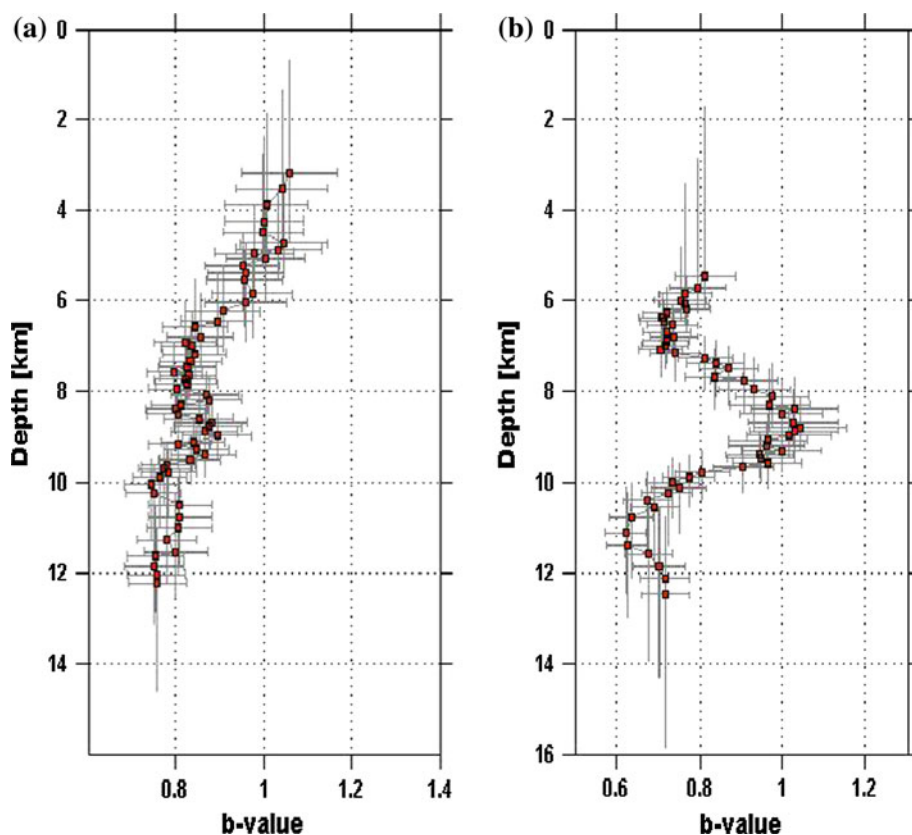

Fig. 12 3D view of b-value at the Bam aftershock area. The mapping is performed in a 0.01° × 0.0.01° × 2 km grid (latitude, longitude and depth), Selecting the nearest 150 events in each node. The N–S vertical section is along the Bam earthquake rupture zone. The three *horizontal* slices are shown at depths of 2, 8 and 12 km. The high b-value anomalies are colored red. *White dots* show the location of aftershock events (data from Sadeghi et al. 2006)

variation of this value may be related to the tectonic condition of earthquake area, such as, material heterogeneity (Mogi 1962), variation of applied stress (Scholz 1968), change in effective pore pressure (Wyss 1973) and thermal gradients (Warren and Latham 1970).

Many studies have been done to describe the spatial distribution of b-value in aftershock sequences. In some of these studies, the FMD is believed to be perturbed by stress and material heterogeneity (Scholz 1990; Urbancic et al. 1992; Wiemer and Wyss 1997; Wiemer et al. 1998; Bayrak and Ozturk 2004).

Wiemer and Katsumata (1999) studied the spatial variability of b and P values in aftershock sequence of M 7.2 Kobe, M6.2 Morgan Hill, M7.2 Landers and M6.7 Northridge earthquakes. By comparing the slip during the main shock with the b-value distribution in all four events, they suggested that near the highest slip release, the applied shear stress drops significantly, favoring a higher b-value for aftershocks. They also pointed out that the applied sheer stress, crack density and pore pressure also govern the magnitude–frequency distribution in an aftershock zone.

As discussed previously, the depth distribution of the average b-value in the Bam aftershock zone shows two significant increases (Fig. 11a, b). One in depths shallower than 4 km beneath Bam city, northern part of rupture zone

Fig. 13 Geological map of the Bam area based on the 1:100,000 geological map, sheet 7,648 prepared by the Geological Society of Iran (1993)
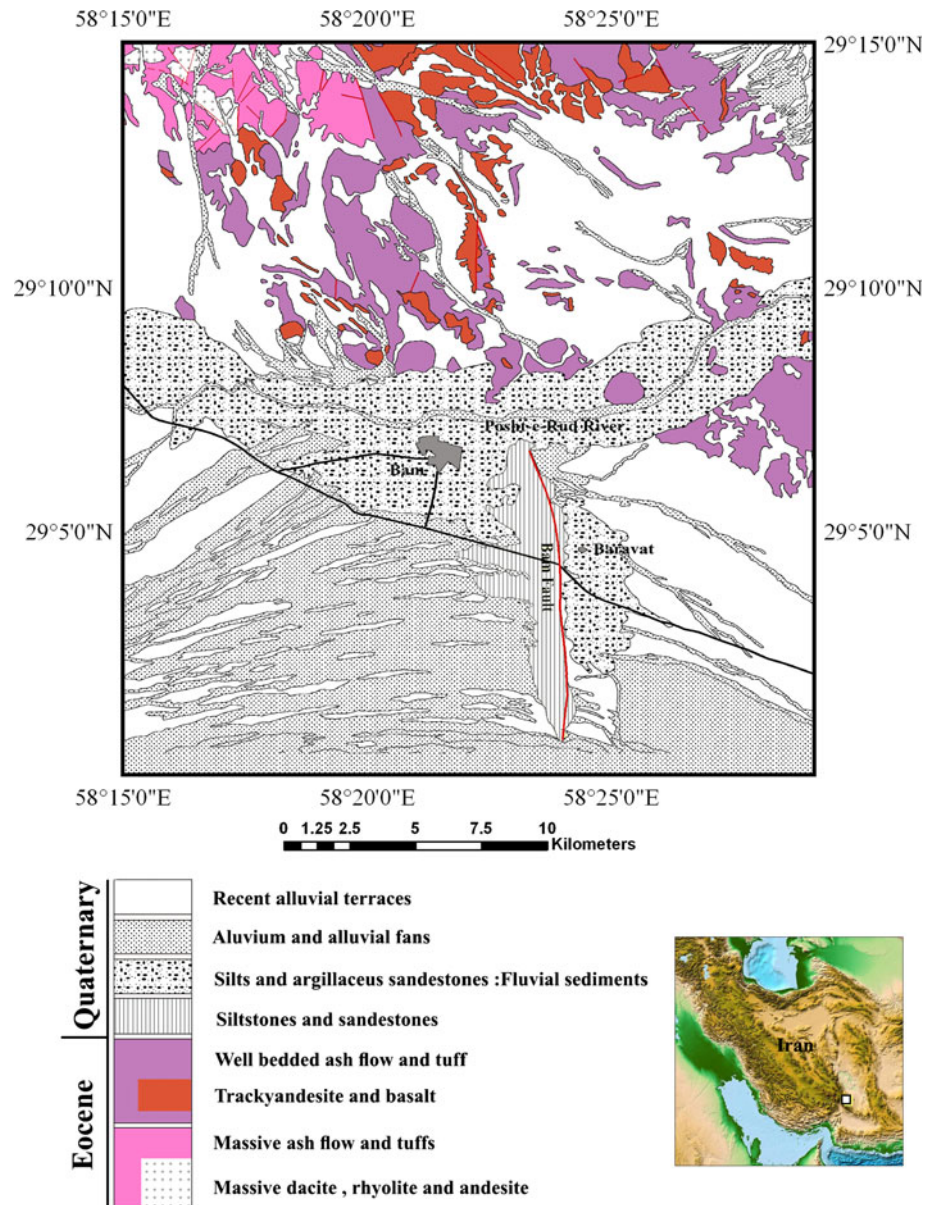
and the second at depth between 8 and 9 km, where the occurrence of aftershocks is also maximum.

As shown in Fig. 7b, the high b-value anomalies in the Bam aftershock zone are not compared with the slip distribution. On the other hand, on the contrary of Wiemer and Katsumata (1999), the area of the largest b-value does not correlate with the area of largest slip that defined by Funning et al. (2005).

The similar observations have been reported by Bayrak and Ozturk (2004) in aftershock zone of the 1999 Izmith and Duzce earthquakes. They interpreted the variation of b-value in this aftershock zone can be related to the stress distribution after the main shock. The higher b-value anomalies correlate with the regions where the lower stress changes occurred. Aktar et al. (2004) studied the spatial

variation of aftershock activity across the rupture zone of the August 17, 1999 Izmit earthquake, Turkey. They detected a high b-value anomaly, which was located beyond rupture zone and interpreted it as a weekend fractured zone. The study of the aftershock pattern of the July 9, 1997, $M_w = 6.9$ Cariaca earthquake by Baumbach et al. (2004) also shows similar results.

The 3D velocity structure of the Bam earthquake area proposed by Sadeghi et al. (2006) revealed a heterogeneous structure for material properties along the Bam rupture zone. This heterogeneity had an important role in controlling b-value variation in Bam aftershock zone.

Sadeghi et al. (2006) marked a thick layer of high V_s and low σ at a depth range of 2 to 6 km and a deeper layer with 2 km thickness, from 6 km to a depth of 9 km beneath the

Bam. The deeper layer shows low V_s and high σ. By comparing the poison's ratio structure and b-value distribution along a cross-section parallel to Arg-e-Bam fault, it reveals that there is a low b-value regions in accordance with high V_s and low σ at the main shock hypocenter and there is high b-value region that may be related to low V_s and high σ below the main shock hypocenter.

Sadeghi et al. (2006) suggested that the increase in Poisson's ratio in depth range 6–10 km may be associated with a change in lithology from rigid and SiO_2-rich rock (at depths 2–6 km) to more mafic ones, perhaps, with existence of fluids (at depths 6–10 km).

As a result, material properties are more important factors in controlling b-value distribution in Bam earthquake rupture zone. The surface high b-value anomaly in the northern part of Bam rupture zone (Anomaly A) may be related to unconsolidated fluvial and water-rich sediment in flood plain of Posht-rud River (Fig. 13) and probable low-strength rocks below these sediments. It is very common because the shallower parts of crust show higher b-value than the deeper parts (Wiemer and Wyss 1997). The deeper anomalies may be related to low V_s–high σ asperity body, which can be a fluid-filled fractured rock masses. Nur and Boocker (1972) proposed a mechanism for aftershock occurrences in shallow earthquakes. They believed that large shallow earthquakes can induce changes in the fluid pore pressure and subsequently redistributed the pore pressure as a result of fluid flow, slowly decreases the strength of rocks and may result in delayed fractures. I believe that this mechanism can be used for describing the aftershock activity of Bam earthquake. I suggested that the pressure of compressed fluids in highly fractured zones played a major role in the development of aftershock activity of the Bam earthquake. The high b-value anomalies beyond the surroundings of high slip area can be correlated with high V_s and low σ materials. Increasing in fluid pore pressure induced by Bam rupture lowered the normal stress in fluid-filled highly fractured materials and modified the coulomb failure criterion for triggering of many small events.

Because of lake of borehole data about the city of Bam, describing the geological properties of deeper high b-value low-velocity asperities is difficult. As shown in the geological map (Fig. 13), the area north of the Bam consists of Eocene volcanic rocks including massive dacite, rhyolite and site, massive tuff, well-bedded volcaniclastic sediments and tuffs. Based on geological structure of Bam area, it can be assumed that the low V_s, high σ asperity body at 6–10 km depth maybe related to extensive fracturing due to volcanism in Eocene. The large heterogeneity in this depth range might have resulted from generation of many fractures due to the movement of magma during its intrusion. These fractures are currently filled by fluid.

Conclusion

In this paper, the b-value of Gutenberg–Richter relation and its spatial variation are investigated for the aftershock sequence of the Bam earthquake. The $Mc = 0.8$ is used in this computation. Mapping the b-value across the bam rupture zone shows the b-value changes between 0.6 and 1.1 in depths. Distribution of b-value in aftershock zone shows two marked increases (1) in depths shallower than 4 km and (2) in depths 8–9 km. The spatial variations across the rupture zone of Bam earthquake revealed that there is no correlation between high b-value and the region of largest slip and larger stress change. There is a good spatial correlation between the high b-value anomalies found in this study and the zone of low V_s and high σ in earlier tomography studies. This correlation reveals that material properties and increasing heterogeneity are important reasons caused by variations of b-value in the Bam aftershock zone. Based on b-value mapping in this study and the earlier tomography studies, the high b-value anomaly near the surface of northern part of rupture zone maybe related to unconsolidated and water-rich quaternary alluvial sediments and probably low strength and highly fractured rocks beneath them. The high b-value anomaly at depth range 8–10 km can be correlated with highly fractured and fluid-filled mass, which may be related to volcanisms in Eocene time. In this study, the induced changes in pore fluid pressure due to main shock are introduced as a mechanism for aftershock generation.

References

Aki K (1965) Maximum likelihood estimate of b in the formula log $N = a - bM$ and its confidence limits. Bull Earthq Res Inst 43:237–239

Aktar M, Ozalaybey S, Ergin M, Karabulut H, Bouin MP, Tapirdamaz C, Bicmen F, Yoruk A, Bouchon M (2004) Spatial variation of aftershock activity across the rupture zone of the 17 August 1999 izmit earthquake, Turkey. Tectonophysics 391:325–334

Baumbach M, Grosser H, Torres GR, Rojas Gonzales JL, Sobiesiak M, Welle W (2004) Aftershock pattern of the July 9, 1997 M_W = 6.9 Cariaco earthquake in Northern Venezuela. Tectonophysics 379:1–23

Bayrak Y, Ozturk S (2004) Spatial and temporal variations of the aftershock sequences of the 1999 İzmit and Duzce earthquakes. Earth Planets Space 56:933–944

Berberian M (1976) Contribution to the seismotectonics of Iran, part II, Materials for the study of the seismotectonics of Iran, Report No. 39, Geological Survey of Iran, Tehran

Binet R, Bollinger L (2005) Horizontal coseismic deformation of the 2003 Bam (Iran) earthquake measured from SPOT-5 THR satellite imagery. Geophys Res Lett 32:L02307. doi:10.1029/2004GL021897

Engdahl ER, Van der Hilst R, Buland R (1998) Global teleseismic earthquake relocation with improved travel times and procedures for depth determination. Bull Seism Soc Am 3:722–743

Fielding EJ, Talebian M, Rosen PA, Nazari H, Jackson JA, Ghorashi M, Walker R (2005) Surface ruptures and building damage of the 2003 Bam, Iran, earthquake mapped by satellite synthetic aperture radar interferometric correlation. J Geophys Res 110: BO3302. doi:10.1029/2004JB003299

Fu B, Ninomiya Y, Lei X, Toda S, Awata Y (2004) Mapping the active strike-slip fault triggered the 2003 Mw 6.6 Bam, Iran, earthquake with ASTER 3D images. Remote Sens Environ 92:153–157

Funning GJ, Parsons B, Wright TJ, Jackson JA, Fielding EJ (2005) Surface displacements and source parameters of the 2003 Bam (Iran) earthquake from Envisat advanced synthetic aperture radar imagery. J Geophys Res 110:B09406. doi:10.1029/2004JB003338

Gutenberg B, Richter CF (1954) Seismicity of the earth. Princeton University Press, Princeton

Hessami K, Tabassi H, Abbassi M, Azuma T, Okumura K, Echigo T, Kondo H (2003) Surface expression of the Bam fault zone in southeastern Iran: causative fault of the December 26, 2003 earthquake. J Seismol Earthq Eng 5:1–10

Ishimoto M, Iida K (1939) Observations of earthquakes registered with the microseismograph constructed recently. Bull Earthq Res Inst Univ Tokyo 17:443–478

Jackson JA, Haines AJ, Holt WE (1995) The accommodation of Arabia–Eurasia plate convergence in Iran. J Geophys Res 100:15205–15219

Mogi K (1962) Magnitude-frequency relation for elastic shocks accompanying fractures of various materials and some related problems in earthquakes. Bull Earthq Res Inst Tokyo Univ 40:831–853

Nakamura T, Suzuki S, Sadeghi H, Fatemi Aghda SM, Matsushima T, Ito Y, Hosseini SK, Gandomi AJ, Maleki M (2005) Source fault structure of the 2003 Bam earthquake, southeastern Iran, inferred from the aftershock distribution and its relation to the heavily damaged area: existence of the Arg-e-Bam fault proposed. Geophys Res Lett 32:L09308. doi:10.1029/2005GL022631

Nur A, Boocker JR (1972) Aftershocks caused by Pore fluid flow. Science 4024:885–887

Sadeghi H, Fatemi Aghda SM, Suzuki S, Nakamura T (2006) 3-D velocity structure of the 2003 Bam earthquake area (SE Iran): existence of a low—poisson's ratio layer and its relation to heavy damage. Tectonophysics 417:269–283

Scholz CH (1968) Microfractures, Aftershocks and seismicity. Bull Seismol Soc Am 58:1117–1130

Scholz CH (1990) The mechanics of earthquakes and faulting. Cambridge University Press, Cambridge, MA

Shi Y, Bolt BA (1982) The standard error of the magnitude-frequency b value. Bull Seism Soc Am 72:1677–1687

Suzuki S, Fatemi Aghda SM, Nakamura T, Matsushima T, Ito Y, Sadeghi H, Maleki M, Gandomi AJ, Hosseini SK (2004) Temporal seismic observation, preliminary hypocenter determination of aftershocks of the 2003 Bam earthquake, southeastern Iran. Bull Earthq Res Inst Univ Tokyo 79:37–45

Talebian M, Fielding EJ, Funning GJ, Ghorashi M, Jackson J, Nazari H, Parsons B, Priestley K, Rosen PA, Walker R, Wright TJ (2004) The 2003 Bam (Iran) earthquake: rupture of a blind strike-slip fault. Geophys Res Lett 31:L11611. doi:10.1029/2004GL020058

Tatar M, Hatzfeld D, Moradi AS, Paul A (2005) The 2003 December 26 Bam earthquake (Iran), Mw 6.6, aftershock sequence. J Int Geophys 163:90–105

Urbancic TI, Trifu CI, Long JM, Young RP (1992) Space-time correlations of b-value with stress release. Pure Appl Geophys 139:449–462

Utsu T (1992) On seismicity, in mathematical seismology(VII), cooperative research report 34. Institute of statistical mathematics, Tokyo, pp 139–157

Utsu T (2002) Statistical features of seismicity, international handbook of earthquake and engineering seismology, vol 81A. IASPEI committee on Education, pp 723–724

Vernant Ph, Nilforoushan F, Hatzfeld D, Abbasi MR, Vigny C, Masson F, Nankali H, Martinod J, Ashtiani A, Bayer R, Tavakoli F, Chéry J (2004) Contemporary crustal deformation and plate kinematics in Middle East constrained by GPS measurements in Iran and northern Oman. Geophys J Int 157:381–398

Walker R, Jackson JA (2002) Offset and evolution of the Gowk fault, S.E. Iran: a major intra-continental strike-slip system. J Struct Geol 24:1677–1698

Warren NW, Latham GV (1970) An experimental study of thermally induced microfracturing and its relation to volcanic seismicity. J Geophys Res 75:4455–4464

Wiemer S, Benoit J (1996) Mapping the b-value anomaly at 100 km depth in the Alaska and New Zealand subduction zones. Geophys Res Lett 23:1557–1560

Wiemer S, Katsumata K (1999) Spatial variability of seismicity parameters in aftershock zones. J Geophys Res 104:13135–13151

Wiemer S, McNutt SR (1997) Variations in the frequency magnitude distribution with depth in two volcanic areas: Mount St. Helens, Washington, and mount Spurr, Alaska. Geophys Res Lett 24:189–192

Wiemer S, Wyss M (1997) Mapping the frequency-magnitude distribution in asperities: an improved technique to calculate reocurrence times. J Geophys Res 102:15115–15128

Wiemer S, Wyss M (2000) Minimum Magnitude of completeness in earthquake catalogues: Examples from Alaska, the Western United States, and Japan. Bull Seism Soc Am 90(4):859–869

Wiemer S, Zuniga RF (1994) ZMAP, a software package to analyze seismicity. EOS Trans Fall Meet AGU 75:456

Wiemer S, McNutt SR, Wyss M (1998) Temporal and three-dimensional spatial analysis of the frequency-magnitude distribution near Long-Valley caldera, California. Geophys J Int 134:409–421

Wiemer S, Gerstenberger MC, Hauksson E (2002) Properties of the 1999, Mw 7.1, Hector mine earthquake: Implications for aftershock hazard. Bull Seism Soc Am 92:1227–1240

Wyss M (1973) Towards a physical understanding of the earthquake frequency distribution. Geophys J R Astronom Soc 31:341–359

Yamanaka Y (2003) Seismological note: No. 145, Earthquake Information Center, Earthquake research institute. University of Tokyo